Applied Catalysis B: Environmental 243 (2019) 614–620

Contents lists available at ScienceDirect

Applied Catalysis B: Environmental

journal homepage: www.elsevier.com/locate/apcatb

Metallic 1T-MoS_2 nanosheets in-situ entrenched on N,P,S-codoped hierarchical carbon microflower as an efficient and robust electro-catalyst for hydrogen evolution

Jie Xiong[a,b,1], Jing Li[a,1], Jiawei Shi[a], Xinlei Zhang[a], Weiwei Cai[a,*], Zehui Yang[a,*], Hansong Cheng[a]

[a] Sustainable Energy Laboratory, Faculty of Materials Science and Chemistry, China University of Geoscinces (Wuhan), 388 Lumo Road, Wuhan, 430074, PR China
[b] College of Chemistry, Chemical Engineering and Materials Science, Zaozhuang University, Zaozhuang, 277160, PR China

ARTICLE INFO

Keywords:
Hydrogen evolution reaction
1T-MoS_2
Hierarchical carbon microflower
P doping
Efficient
Robust

ABSTRACT

Phosphorus contained metallic 1T-MoS_2 produced from *in-situ* ammonium intercalation induced surface sulfur atom distortion of MoS_2 rooted in N,P,S-codoped hierarchical flowerlike carbon (HCMF) hybrids were successfully prepared *via* a dopamine self-polymerization together with molybdate process followed by a hydrothermal reduction route. On account of the coupling effect of metallic phase, defect-rich character, heteroatomic dopants and highly conductive carbon support, the P-MoS_2@HCMF demonstrates prominent performances with an overpotential of merely 86 mV to deliver a current density of 10 mA cm^{-2} and a small Tafel slope of 42.35 mV dec^{-1} for hydrogen evolution reaction (HER) in 0.5 M H_2SO_4, which are among the best results for molybdenum disulfide based HER catalysts. Strikingly, benefiting from S vacancies and P dopant functioning as electron donors, as well as strain arisen from the tensile of rigid carbon microflower scaffold to MoS_2 nanosheets to overcome agglomeration barriers of nanosheets, P-MoS_2@HCMF remained well the pristine 1 T phase and exhibited superior cycling stability with indistinguishable overpotential decay over 5000 sweeps and extraordinary HER durability during the 100 h long-term operation with negligible current deterioration. These findings highlight the prospective potential of P-MoS_2@HCMF as a highly efficient and stable noble metal-free electrocatalyst towards HER.

1. Introduction

Hydrogen is a potentially promising alternative energy carrier to traditional fossil fuel in virtue of its renewability, environmental friendliness and highest mass-specific energy density [1,2]. For clean and sustainable hydrogen production, the electrochemical catalytic hydrogen evolution reaction (HER) *via* splitting water using renewable electrical energy is believed to be a safe and efficient process among all the hydrogen generation approaches, which requires advanced catalysts to minimize the dynamic overpotential [3,4]. Pt-group metals are well established to be the state-of-the-art benchmark electrocatalyst towards HER [5–7], nevertheless, their low earth-abundance and corresponding high cost impede the scale-up application [8–11]. As a consequence, cost-effective transition metal sulfides [8,12–17], carbides [3,18–23], phosphates [4,10,24–28], nitrides [1,29–32] and borides [33] with varied nanomorphologies have been extensively investigated for efficient and stable HER catalysis.

Molybdenum disulfide (MoS_2), a typical layered transition metal dichalcogenide (TMD), has attracted increasing attention in energy conversion field due to its clearly elucidated active sites stemming from the S defects exposed on the edge of MoS_2 and highly active electrocatalytic performance [34]. Inspired by this understanding, 2H-MoS_2 nanosheets with abundant defects or/and small sizes to favor maximal exposure of active edge sites have been well-explored for efficient electricity-driven hydrogen production [8]. It seems, however, that improving the HER activity of 2H-MoS_2 by means of exposing reactive edges has encountered the bottleneck because of its extremely low interplanar conductivity, specifically, which is 2200-fold less than that along the direction parallel to basal plane, is another intrinsic performance-limiting factor [35]. Metallic 1 T-MoS_2, distinguished from the semiconducting 2H-MoS_2, which exhibits much better electrochemical activity than its 2H phase counterpart on account of its abundant

* Coressponding authors.
E-mail addresses: willcai1985@gmail.com (W. Cai), yeungzehui@gmail.com (Z. Yang).
[1] These authors contributed equally.

https://doi.org/10.1016/j.apcatb.2018.11.004
Received 3 July 2018; Received in revised form 26 October 2018; Accepted 2 November 2018
Available online 03 November 2018
0926-3373/

catalytically active sites from edges and basal plane in addition to its rapid electron transfer rate [35–43]. Whereas, 1 T-MoS_2 is a thermodynamically metastable phase that is prone to undergo an irreversible transition to the more stable 2H phase owing to the S-S van der Waals interactions [36,38,40,41,44,45]. Fortunately, this issue could be addressed by introducing proper dopants possessing electron-donor capability into the 1 T system, and 1 T-MoS_2 have been reported to be effectively stabilized by incorporating of Re [46,47], Au [46–48], Tc [36] atoms and Ni-Co complexes [49], which act as electron donors to impose stabilization effect on 1 T-MoS_2 by assurance the high electron density in the d orbital of molybdenum ions. Moreover, both the theoretical calculation based on density functional theory (DFT) and experimental results reveal that 1 T phase becomes more stable in the presence of injected electron or under negatively charged circumstances [45,47,50–53]. Very recently, an encouraging strategy *via* introducing S vacancies, which actually acted as a source of electron donor, to stabilize 1 T-MoS_2 by plasma irradiation [54] and hydrothermal Li^+ intercalation followed by exfoliation [44] are also proposed. Notably, how to fabricate a phase stable and morphologically invariable metal-like MoS_2 nanosheet towards promoted hydrogen evolution reaction is still highly desirable because the nanosheets are tended to aggregate and stack together due to its high surface energy [9,55] apart from the abovementioned instability of 1 T phase.

Here in this work, a facile strategy for *in*-situ growing of ultrastable P contained metallic MoS_2 nanosheets on N,P,S-codoped hierarchical carbon microflower (P-MoS_2@HCMF as illustrated in Scheme 1) was proposed, in which ammonium in thiourea and ammonium dihydrogen phosphate serving as the intercalation agent was used to trigger the lateral sliding of surface S-layer of MoS_2 anchored on the carbon microflower scaffold and thus activate the 2H to 1 T phase transition as well as creating certain S vacancies. Owing to the cooperative effect of metallic phase, defective feature, heteroatomic dopants and highly conductive carbon support, the P-MoS_2@HCMF demonstrated excellent performances with an ultralow η_{10} value (defined as the HER overpotential to generate a cathodic current density of 10 mA cm^{-2}) of 86 mV and a small Tafel slope of 42.35 mV dec^{-1} in 0.5 M H_2SO_4. Noticeably, stabilized by S vacancies and P dopant acting as electron donors, as well as strain originated from the tensile of rigid carbon microflower framework to MoS_2 nanosheets to get rid of stacking of nanosheets, P-MoS_2@HCMF maintained well the initial 1 T metal phase and exhibited outstanding HER durability during the 100 h long-term operation with undetectable current loss.

2. Experimental

2.1. Materials

All chemicals were of reagent grade and used as received without further purification. Ammonium molybdate tetrahydrate ($(NH_4)_6Mo_7O_{24}{\cdot}4H_2O$), thiourea ($CH_4N_2S$), ammonium dihydrogen phosphate ($NH_4H_2PO_4$), dopamine hydrochloride ($C_8H_{11}NO_2{\cdot}HCl$) and 5 wt% Nafion solution were purchased from Sigma-Aldrich. The anhydrous ethanol, ammonia hydroxide ($NH_3{\cdot}H_2O$) and concentrated sulfuric acid (H_2SO_4, 98 wt%) were provided by Sinopharm Chemical Reagent Co., Ltd., China. The filter membrane (Celgard, USA), commercial 20 wt% Pt/C catalyst, Vulcan XC-72R carbon black, glassy carbon (GC) electrode, saturated calomel electrode (SCE) and graphite rod (99.9995%) were offered by Alfa Aesar. All solutions were prepared using deionized water produced from a water purifier (Milli-Q, USA).

2.2. Synthesis of P-MoS_2 @HCMF catalysts

Briefly, 1.236 g (1 mmol) of $(NH_4)_6Mo_7O_{24}{\cdot}4H_2O$ powder was dissolved in 60 mL of deionized water and 26 mL of absolute ethanol under vigorously magnetic stirring for 30 min to form homogeneous solution, whose pH was then adjusted to around 8 with the introduction of 1.3 mL of $NH_3{\cdot}H_2O$, followed by a dropwise addition of 33 mL of 20 mg mL^{-1} dopamine, which is widely used as carbon source [56], solution into the above suspension. After on-going stirring and further reaction for 10 h, a dark red precursor dispersion was formed, during which dopamine molecules gradually self-polymerized and assembled into hierarchical microflower architecture carbon taking along chelated Mo ions under weakly alkaline condition. Subsequently, the obtained Mo precursor dispersion was filtered through a Celgard membrane and rinsed repetitively with deionized water and ethanol, and then dried. The collected Mo-polydopamine powder was thereafter subject to a carbonization procedure under Ar gas maintained at 600 °C for 2 h at a slow heating ramp of 2 °C min^{-1}. After cooling down, it was dispersed into 35 mL of deionized water along with 4.568 g of thiourea and 34.51 mg (0.3 mmol) of $NH_4H_2PO_4$ under continuous magnetically stirring for 1 h, which was then transferred into a Teflon-lined stainless steel autoclave with a capacity of 50 mL and undergone a 20 h hydrothermal treatment at 220 °C. Finally, the harvested products were filtered and washed thoroughly with Milli-Q water and ethanol to remove any possible impurities and dried at 60 °C for 2 h to obtain P-MoS_2@HCMF powders. For comparison, various contents of 11.50 mg (0.1 mmol) and 57.52 mg (0.5 mmol), respectively, of $NH_4H_2PO_4$ were also employed, and the correspondingly obtained catalysts were denoted as P-MoS_2-0.1@HCMF and P-MoS_2-0.5@HCMF.

Details on material characterizations and electrochemical measurements are provided in Supporting Information.

3. Results and discussion

The X-ray diffraction patterns of the as-obtained P-MoS_2@HCMF and MoS_2@HCMF without P doping were presented in Fig. 1a. Distinct peaks indexed as standard MoS_2 (JCPDS NO. 37-1492) at 32.68° and 58.33°, corresponding to the (100) and (110) crystal planes of MoS_2, respectively, can be detected from both spectra, confirming the successful synthesis of MoS_2 in both catalysts. Moreover, the absence of

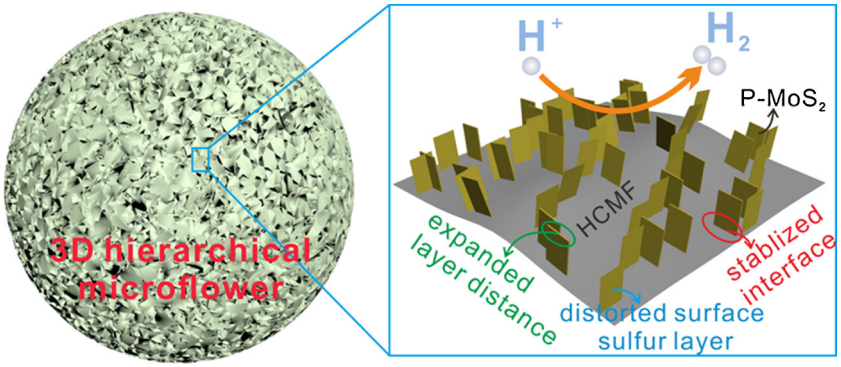

Scheme 1. Schematic diagram of the P-MoS_2@HCMF catalysts.

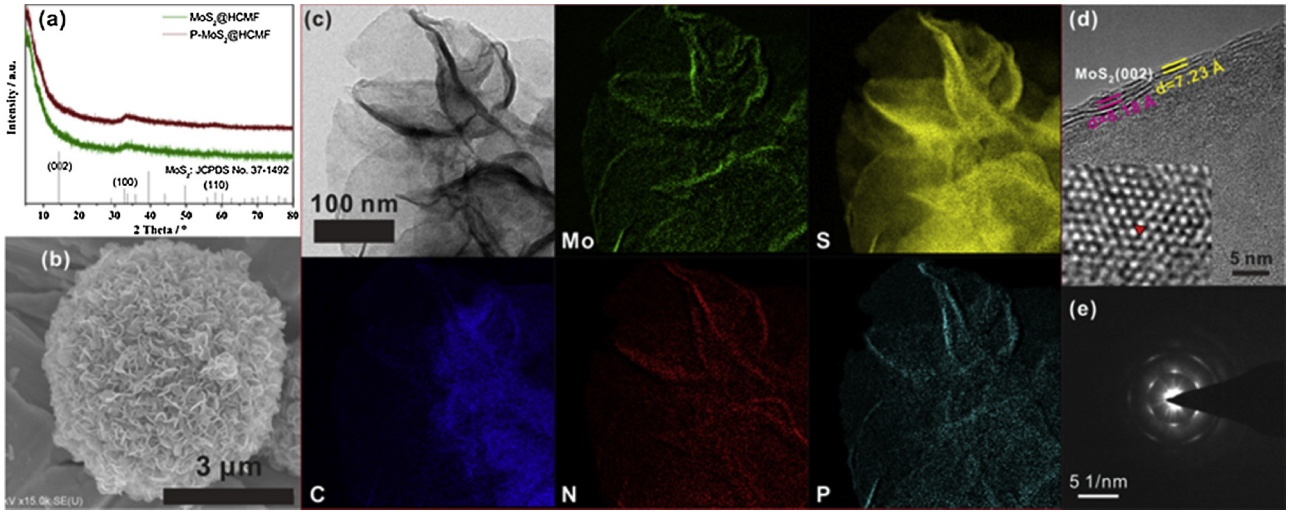

Fig. 1. (a) The XRD patterns of MoS_2@HCMF and P-MoS_2@HCMF catalysts; (b) SEM image; (c) TEM image and corresponding EDS elemental mappings; (d) HR-TEM image and (e) SAED pattern of P-MoS_2@HCMF.

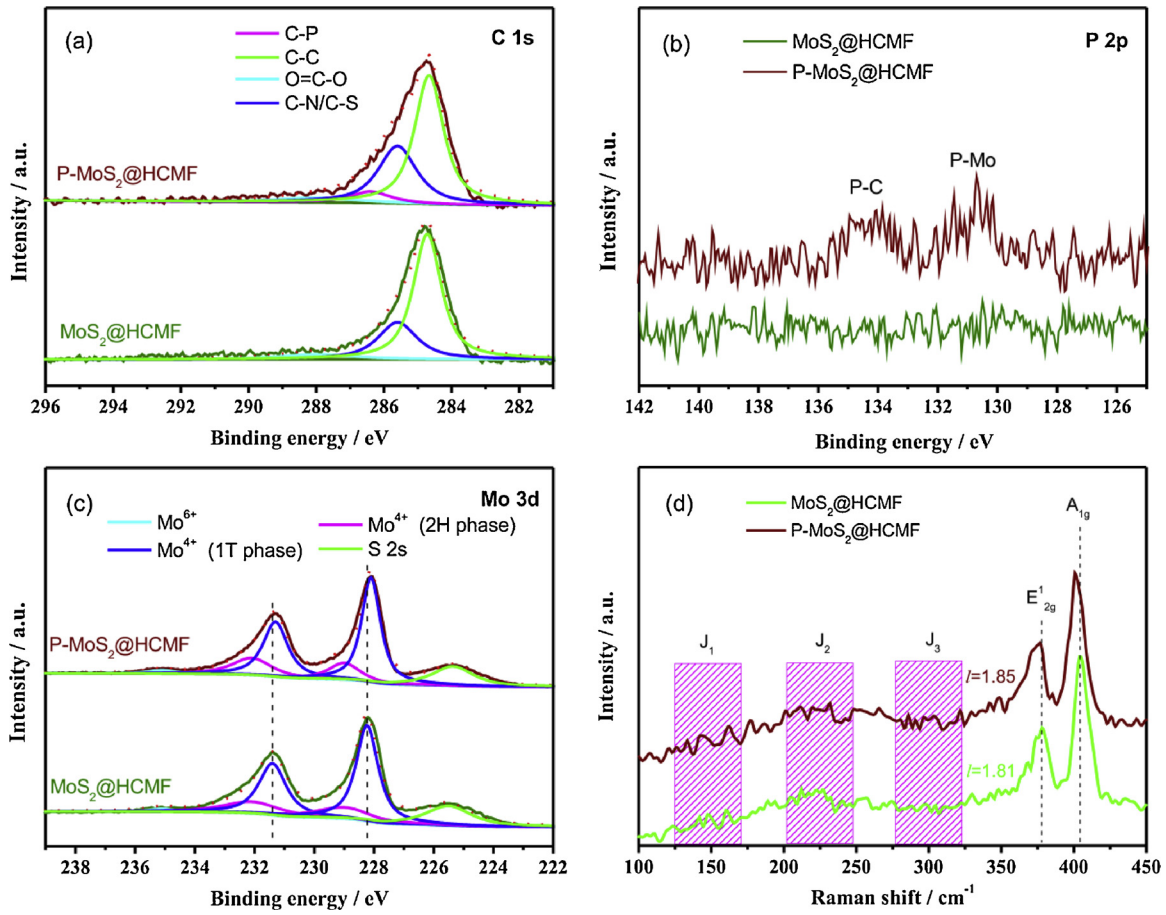

Fig. 2. High-resolution XPS spectra of (a) C 1 s, (b) P 2p and (c) Mo 3d; (d) Raman spectra of the MoS_2@HCMF and P-MoS_2@HCMF catalysts.

(002) plane located at 14.38° indicates few-layer characteristic of MoS_2 nanosheets as elucidated in previous literatures [55,57]. Scanning electron microscopy (SEM) image of the P-MoS_2@HCMF (Fig. 1b) reveals the successful retention of the 3D architecture microflower morphology of the carbonized Mo-polydopamine and pristine MoS_2@HCMF without P doping (Fig. S1). Size of the P-MoS_2@HCMF is large to 3–4 μm, allowing the loose and radiating growth of MoS_2 nanosheets on the petals of flowerlike carbon. The observed wrinkled structure with crumpled edges and high transparency of the transmission electron microscopy (TEM) profile of the P-MoS_2@HCMF as displayed in Fig. 1c illustrates the ultrathin feature of the MoS_2 nanoflakes. The corresponding energy dispersive spectrum (EDS) elemental mappings reveal that the P-MoS_2@HCMF is predominantly composed of Mo, S and C elements, and the N, P heteroatoms, which are inherited from the amine functionality in dopamine molecule and phosphate group in ammonium dihydrogen phosphate, respectively, are uniformly distributed in the

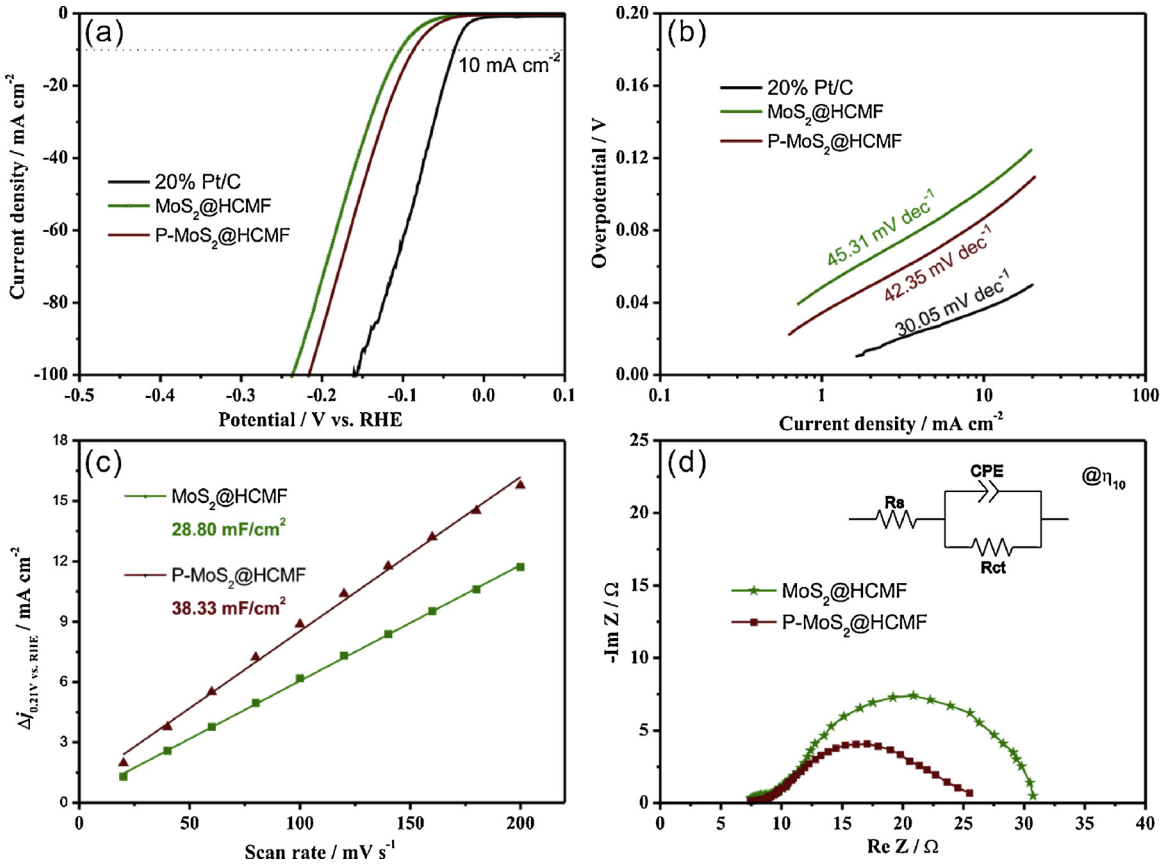

Fig. 3. (a) Polarization curves, (b) corresponding Tafel curves, (c) electrochemical double-layer capacitances and (d) electrochemical impedance spectroscopy (inset: equivalent circuit) of HER on the MoS_2@HCMF and P-MoS_2@HCMF catalysts in 0.5 M H_2SO_4.

composite. According to the high-resolution transmission electron microscopy (HR-TEM) image shown in Fig. 1d, expanded interlayer spacing around 0.80 nm for P-MoS_2@HCMF are detected compared to that of common MoS_2 nanosheets which is usually described to be 0.62 nm [55,57]. The enlargement of MoS_2 interplanar distance between two adjacent (002) planes suggests the existence of metallic 1 T-MoS_2 in P-MoS_2@HCMF, which is further corroborated by the trigonal lattice arrangement of octahedral coordination for the 1 T phase MoS_2 [44,48] as depicted in the inset of Fig. 1d. The formation of metallic 1 T phase was caused by the intercalating of ammonium resulted from the strong coordination bonding of the transition metal centers of Mo with the nitrogen atoms from thiourea and ammonium dihydrogen phosphate molecules [58], the large size of intercalated species would lead to the transversal distortion of surface sulfur atoms in MoS_2 immobilized on the flowerlike carbon substrate and initiate the desirable 2H to 1 T phase change, meanwhile, generating some S vacancies due to certain surface S atoms inevitably escape from the lattice during the intercalation process. Note that numerous crystal fringes are discontinuous in Fig. 1d, indicating the existence of abundant defects, which is further manifested by the selected area electron diffraction (SAED) pattern (Fig. 1e) in the form of six independent diffraction arcs, a representative quasiperiodic structure with rich defects [8,31]. Moreover, it's evidently that the number of lamina in a single MoS_2 nanosheet along the (002) crystal plane is 3–4 layers, agreeing well with the few-layer structure identified by the aforementioned XRD results.

To provide more information on the composition and chemical bonding states, X-ray photoelectron spectroscopy (XPS) analysis was performed. In the fitted XPS C 1 s core level spectrum of MoS_2@HCMF (Fig. 2a), the main peak positioned at ~284.6 eV is assigned to the sp^2 hybridized graphitic carbon, the peak centered at 285.6 eV is attributed to C–N and C–S, while the broad band with low intensity at 288.0 eV is ascribed to O = C–O [59,60]. For P-MoS_2@HCMF, the additional resonance located at 286.4 eV belongs to C–P bond [60]. The deconvoluted P 2p region of P-MoS_2@HCMF as illustrated in Fig. 2b is composed of two contributions from both P—C (134.0 eV) [2,61] and P-Mo (130.5 eV) [2]. These results validate the successful doping of N, P and S elements into the carbon framework, and the formed P-Mo bonds will certainly modify the electronic configurations of MoS_2. The corresponding XPS quantitative measurement results are listed in Table S1, revealing a P content of 0.64 atm.% in P-MoS_2@HCMF, and the S vacancy concentration is found to increase from 2.08% for MoS_2@HCMF to 9.61% for P-MoS_2@HCMF on the basis of calculation of the S/Mo molar ratio. Besides, the mass fractions of MoS_2 in the hybrids are evaluated to be 76.73% and 77.72%, respectively, for MoS_2@HCMF and P-MoS_2@HCMF, consistent with the estimated proportions based on thermogravimetry (TG) analysis as exhibited in Fig. S2 by assuming the MoS_2 are thoroughly oxidized to MoO_3. The deconvolution of high-resolution Mo 3d signals for MoS_2@HCMF (Fig. 2c) reveals a doublet of predominantly characteristic 1 T phase peaks of Mo $3d_{3/2}$ and Mo $3d_{5/2}$ located at 231.4 eV and 228.2 eV, which are much lower than that of their 2H phase counterparts (232.1 eV and 229.0 eV). Similar downward movement of binding energies of 0.7-0.8 eV for S 2p as shown in Fig. S3 provides the same evidence on the formation of metallic 1 T phase MoS_2. As for P-MoS_2@HCMF, whose Mo 3d resonances exhibit a further downshift to lower binding energies, suggesting the enriched electrons around Mo in P-MoS_2@HCMF. Such variation should be attributed to the lower electronegativity of P compared with S, and as a consequence, reducing the electron transport from Mo when S is partially substituted by P, resulting in considerable negative charges on the surface of catalyst. The increase of S vacancies and electron density around the surface of Mo for the P-MoS_2@HCMF would surely improve the stability of 1 T phase MoS_2. Further quantitative analysis of the

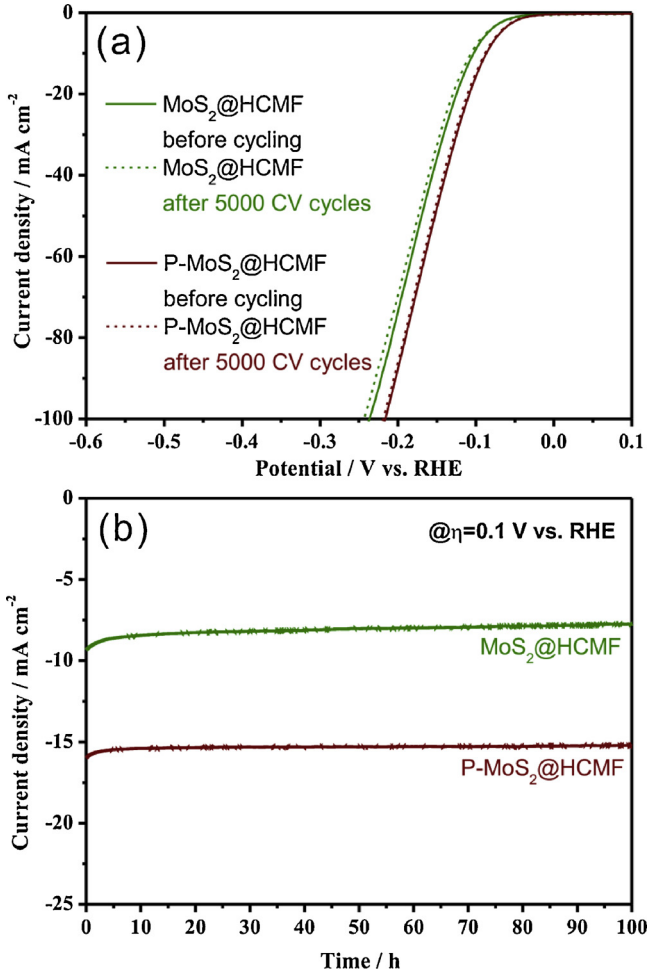

Fig. 4. (a) Long-term cycling stability and (b) Time-dependent profiles of HER current density on MoS_2@HCMF and P-MoS_2@HCMF at the overpotential of 0.1 V under acid condition.

phase composition based on the deconvoluted Mo 3d resonances reveal that the contents of 1 T phase are 73.63% and 74.38%, respectively, in MoS_2@HCMF and P-MoS_2@HCMF. Raman spectroscopy was conducted to confirm the structure and assess the strain in the P-MoS_2@HCMF. As demonstrated in Fig. 2d, the J_1, J_2 and J_3 phonon modes derived from the superlattice structure of 1 T phase MoS_2 [47], and the high intensity ratio (*i.e.*, *l*) of A_{1g} (out-of-plane vibration) to E^1_{2g} (in-plane vibration) reflects its edge-terminated characteristic of MoS_2@HCMF and P-MoS_2@HCMF [62], which originates from its ultrathin few-layer structure and defect-rich nature as illustrated in Fig. 1. Moreover, the E^1_{2g} and A_{1g} modes of P-MoS_2@HCMF, which are highly sensitive to tensile or compressive strain, are slightly red-shifted, demonstrating the presence of tensile stress in P-MoS_2@HCMF [63]. The tensile strain coming from the attempts of robust flowerlike carbon backbone prevents the MoS_2 nanoflake grown on it from restacking together, which is also believed to be greatly advantageous for the preservation of 1 T phase MoS_2 by maintaining the distortion of surface sulfur layer.

The electrocatalytic HER performances of MoS_2@HCMF and P-MoS_2@HCMF under acidic condition is subsequently investigated and compared in Fig. 3a-b with those of benchmark commercial 20% Pt/C by depositing the catalysts with the same mass loading of 0.285 mg cm^{-2} on a glassy carbon electrode. Although Pt/C catalyst behaves best among all the three candidates in regard to onset potential, operating overpotential and Tafel slope, the MoS_2@HCMF exhibits competitive reaction activity just requiring an overpotential of 103 mV to drive a current density of 10 mA cm^{-2} (η_{10}) and striking electrode metrics with a small Tafel slope of 45.31 mV dec^{-1}. Encouragingly, the P-MoS_2@HCMF demonstrated even better catalytic performances with an ultralow η_{10} of 86 mV and a smaller Tafel slope of 42.35 mV dec^{-1}, implying the positive role of P playing for HER. The small Tafel slope value is approaching to the theoretical value of 40 mV dec^{-1} for the hydrogen evolution reaction proceeding through the Volmer-Heyrovsky mechanism in which the electrochemical desorption of hydrogen is the rate-determining step. Interestingly, further increasing in P content seemed to be of no significant effect upon the enhancement of HER performance (Fig. S4). Delightedly, these performances are ranked the best ever reported values for MoS_2 based HER electrocatalysts (Table S2). Moreover, the high electrochemical double-layer capacitance (C_{dl}, Fig. 3c) of 38.33 m F cm^{-2} for P-MoS_2@HCMF determined by the cyclic voltammetry (CV) method (Fig. S5) indicates a large electrochemical active surface area (ECSA) for HER and the low charge transfer resistance (R_{ct}) of just 18.6 Ω obtained from Nyquist plots of electrochemical impedance spectroscopy (EIS) conducted at given potential of η_{10} (Fig. 3d) implies the rapid electron diffusion, which is in accordance with its brilliant HER performance, due to that electron hopping only occurs between the metallic 1 T domains [64]. Associating with the aforementioned physicochemical characterizations, the unprecedented HER electrocatalytic activity of P-MoS_2@HCMF hybrid could be attributed to the following aspects: (i) the proliferated negative charges around molybdenum ions induced by the incorporation of P actually functioning as electron donor compared to S with higher electronegativity, which not only facilitates their reaction with H^+ to form adsorbed hydrogen atoms (H_{ads}) but also weakens the H atom binding energy, resulting that the hydronium ions are more easily adsorbed and meanwhile H_{ads} are less difficultly released from the catalyst surface of P-MoS_2@HCMF during the electrochemical hydrogen evolution process to produce H_2 efficiently; (ii) the maximally exposed active sites of 1 T phase MoS_2 since both its edges and basal plane are catalytically active as well as its few layer defect-abundant character; (iii) the combination of metallic 1 T phase MoS_2 and highly conductive carbon substrate renders the improved charge transfer and mass transport as well as the favorable synergistic effect between P doped MoS_2 and N,P,S-codoped hierarchical carbon microflower while HER activity of heteroatom-doped carbon materials has been widely proved [65,66]; (iv) the atomic thin MoS_2 nanoflakes separately stabilized on the 3D hierarchically open carbon framework allows the full access of the electrolyte and endows a shortened electron and ion diffusion path in the solid, liquid and gas contacted triple-phase boundary.

Durability is an indispensable concern for the practical application of a HER catalyst. After 5000 cycles of CV sweeping, there are no remarkable performance loss for MoS_2@HCMF with the ignorable increment in η_{10} and η_{100} as low as 3.1 mV and 7.0 mV, respectively, as demonstrated in Fig. 4a, which indicates the existence of S vacancies and strain are significantly beneficial to the stability of metallic 1 T-MoS_2. As expected, the P-MoS_2@HCMF exhibited even better long-term cycling stability with more inappreciable η_{10} and η_{100} increment of 1.9 mV and 2.8 mV after CV examination, respectively. Definitely, the enriched electron density around molybdenum ions triggered by the introduction of P actually serving as electron donor compared to more electronegative S as well as the increased S vacancies in addition to the tensile stress from rigid carbon scaffold are responsible for the improved stability. Accordingly, the durability results of I-t chronoamperometric (CA) response in 0.5 M H_2SO_4 for MoS_2@HCMF and P-MoS_2@HCMF (Fig. 4b) carried out at an overpotential of 0.1 V over 100 h are identical to that of cycling stability, and the P-MoS_2@HCMF displays a visibly smoother profile than that of MoS_2@HCMF. Besides, no changes are observed from the high resolution XPS Mo 3d signals after the durability testing as shown in Fig. S6, indicating the prominent durability of P-MoS_2@HCMF and a bright prospect for highly efficient and stable HER catalysis.

4. Conclusions

In summary, we designed and developed a novel approach to synthesize metallic P-MoS_2@HCMF hybrid catalysts *via* combining a dopamine self-assembling into flowerlike carbon sphere together with molybdate process and a following *in situ* hydrothermal reduction strategy, during which thiourea acted as the strong reductant as well as an intercalator to incur the horizontal displacement of surface S-layer of MoS_2 planted on the carbon microflower scaffold inducing the 2H to 1 T phase transformation as well as creation of certain S vacancies. Thanks to the synergistic effect of metallic phase, defective structure, heteroatomic dopants and highly conductive carbon support, the P-MoS_2@HCMF behaved splendid electrochemical HER performance requiring an overpotential of only 86 mV to yield a current density of 10 mA cm^{-2} in 0.5 M H_2SO_4 and striking kinetic metrics with a small Tafel slope of 42.35 mV dec^{-1}. Remarkably, by reason of S vacancies and P dopant playing roles as electron donors, as well as stress stemming from the tensile of rigid carbon microflower backbone to MoS_2 nanosheets to prevent their agglomeration and stacking tendency, the P-MoS_2@HCMF well preserved the original 1 T metal phase and exhibited an impressive chronoamperometric (I-t) durability during a 100 h continuous HER operation and also a brilliant cycling stability with unobservable overpotential degradation after 5000-cycle CV examination. These performances are all among the best reported ones, revealing promising application potential for P-MoS_2@HCMF towards HER.

Acknowledgment

We are grateful for financial support from the National Natural Science Foundation of China (Nos. 21875224, 21703211, 21503197 and 21703212).

Appendix A. Supplementary data

Supplementary material related to this article can be found, in the online version, at doi:https://doi.org/10.1016/j.apcatb.2018.11.004.

References

[1] Y. Zhang, B. Ouyang, J. Xu, S. Chen, R.S. Rawat, H.J. Fan, 3D porous hierarchical nickel-molybdenum nitrides synthesized by RF plasma as highly active and stable hydrogen-evolution-reaction electrocatalysts, Adv. Energy Mater. 6 (2016) 1600221.
[2] Z. Shi, K. Nie, Z.-J. Shao, B. Gao, H. Lin, H. Zhang, B. Liu, Y. Wang, Y. Zhang, X. Sun, X.-M. Cao, P. Hu, Q. Gao, Y. Tang, Phosphorus-Mo2C@carbon nanowires toward efficient electrochemical hydrogen evolution: composition, structural and electronic regulation, Energy Environ. Sci. 10 (2017) 1262–1271.
[3] H.B. Wu, B.Y. Xia, L. Yu, X.-Y. Yu, X.W. Lou, Porous molybdenum carbide nano-octahedrons synthesized via confined carburization in metal-organic frameworks for efficient hydrogen production, Nat. Commun. 6 (2015) 6512.
[4] Z. Pu, X. Ya, I.S. Amiinu, Z. Tu, X. Liu, W. Li, S. Mu, Ultrasmall Tungsten Phosphide Nanoparticles Embedded in Nitrogen-Doped Carbon as a Highly Active and Stable Hydrogen-Evolution Electrocatalyst, J. Mater. Chem. A Mater. Energy Sustain. 4 (2016) 15327–15332.
[5] R. Kumar, R. Rai, S. Gautam, A. De Sarkar, N. Tiwari, S.N. Jha, D. Bhattacharyya, A.K. Ganguli, V. Bagchi, Nano-structured hybrid molybdenum carbides/nitrides generated in situ for HER applications, J. Mater. Chem. A Mater. Energy Sustain. 5 (2017) 7764–7768.
[6] L. Zhang, J. Lu, S. Yin, L. Luo, S. Jing, A. Brouzgou, J. Chen, P.K. Shen, P. Tsiakaras, One-pot synthesized boron-doped RhFe alloy with enhanced catalytic performance for hydrogen evolution reaction, Appl. Catal. B 230 (2018) 58–64.
[7] H. Lv, X. Chen, D. Xu, Y. Hu, H. Zheng, S.L. Suib, B. Liu, Ultrathin PdPt bimetallic nanowires with enhanced electrocatalytic performance for hydrogen evolution reaction, Appl. Catal. B 238 (2018) 525–532.
[8] J. Xie, H. Zhang, S. Li, R. Wang, X. Sun, M. Zhou, J. Zhou, X.W. Lou, Y. Xie, Defect-rich MoS2 ultrathin nanosheets with additional active edge sites for enhanced electrocatalytic hydrogen evolution, Adv. Mater. 25 (2013) 5807–5813.
[9] Y. Huang, Q. Gong, X. Song, K. Feng, K. Nie, F. Zhao, Y. Wang, M. Zeng, J. Zhong, Y. Li, Mo2C nanoparticles dispersed on hierarchical carbon microflowers for efficient electrocatalytic hydrogen evolution, ACS Nano 10 (2016) 11337–11343.
[10] X. Zhang, X. Zhang, H. Xu, Z. Wu, H. Wang, Y. Liang, Iron-doped cobalt monophosphide nanosheet/carbon nanotube hybrids as active and stable electrocatalysts for water splitting, Adv. Funct. Mater. 27 (2017) 1606635.
[11] H. Tan, Y. Li, X. Jiang, J. Tang, Z. Wang, H. Qian, P. Mei, V. Malgras, Y. Bando, Y. Yamauchi, Perfectly ordered mesoporous iron-nitrogen doped carbon as highly efficient catalyst for oxygen reduction reaction in both alkaline and acidic electrolytes, Nano Energy 36 (2017) 286–294.
[12] J. Xie, H. Qu, J. Xin, X. Zhang, G. Cui, X. Zhang, J. Bao, B. Tang, Y. Xie, Defect-rich MoS_2nanowall catalyst for efficient hydrogen evolution reaction, Nano Res. 10 (2017) 1178–1188.
[13] J. Wang, M. Yan, K. Zhao, X. Liao, P. Wang, X. Pan, W. Yang, L. Mai, Field effect enhanced hydrogen evolution reaction of MoS_2nanosheets, Adv. Mater. 29 (2017) 1604464.
[14] D. Kong, H. Wang, J.J. Cha, M. Pasta, K.J. Koski, J. Yao, Y. Cui, Synthesis of MoS_2 and $MoSe_2$ films with vertically aligned layers, Nano Lett. 13 (2013) 1341–1347.
[15] Y. Li, H. Wang, L. Xie, Y. Liang, G. Hong, H. Dai, MoS2 nanoparticles grown on graphene: an advanced catalyst for the hydrogen evolution reaction, J. Am. Chem. Soc. 133 (2011) 7296–7299.
[16] Y. Ling, Z. Yang, Q. Zhang, Y. Zhang, W. Cai, H. Cheng, A self-template synthesis of defect-rich WS2 as a highly efficient electrocatalyst for the hydrogen evolution reaction, Chem. Commun. 54 (2018) 2631–2634.
[17] Y. Guo, J. Tang, H. Qian, Z. Wang, Y. Yamauchi, One-pot synthesis of zeolitic imidazolate framework 67-derived hollow Co3S4@MoS2 heterostructures as efficient bifunctional Catalysts, Chem. Mater. 29 (2017) 5566–5573.
[18] C. Lu, D. Tranca, J. Zhang, Fn. Rodríguez Hernández, Y. Su, X. Zhuang, F. Zhang, G. Seifert, X. Feng, Molybdenum carbide-embedded nitrogen-doped porous carbon nanosheets as electrocatalysts for water splitting in alkaline media, ACS Nano 11 (2017) 3933–3942.
[19] J.-S. Li, Y. Wang, C.-H. Liu, S.-L. Li, Y.-G. Wang, L.-Z. Dong, Z.-H. Dai, Y.-F. Li, Y.-Q. Lan, Coupled molybdenum carbide and reduced graphene oxide electrocatalysts for efficient hydrogen evolution, Nat. Commun. 7 (2016) 11204.
[20] J. Xiong, J. Li, J. Shi, X. Zhang, N.-T. Suen, Z. Liu, Y. Huang, G. Xu, W. Cai, X. Lei, L. Feng, Z. Yang, L. Huang, H. Cheng, In situ engineering of double-phase interface in Mo/Mo2C heteronanosheets for boosted hydrogen evolution reaction, ACS Energy Lett. 3 (2018) 341–348.
[21] L. Liao, S. Wang, J. Xiao, X. Bian, Y. Zhang, M.D. Scanlon, X. Hu, Y. Tang, B. Liu, H.H. Girault, A nanoporous molybdenum carbide nanowire as an electrocatalyst for hydrogen evolution reaction, Energy Environ. Sci. 7 (2014) 387–392.
[22] S. Wang, J. Wang, M. Zhu, X. Bao, B. Xiao, D. Su, H. Li, Y. Wang, Molybdenum-carbide-Modified nitrogen-doped carbon vesicle encapsulating nickel nanoparticles: a highly efficient, low-cost catalyst for hydrogen evolution reaction, J. Am. Chem. Soc. 137 (2015) 15753–15759.
[23] Y. Guo, J. Tang, J. Henzie, B. Jiang, H. Qian, Z. Wang, H. Tan, Y. Bando, Y. Yamauchi, Assembly of hollow mesoporous nanoarchitectures composed of ultrafine Mo2C nanoparticles on N-doped carbon nanosheets for efficient electrocatalytic reduction of oxygen, Mater. Horiz. 4 (2017) 1171–1177.
[24] R. Zhang, X. Wang, S. Yu, T. Wen, X. Zhu, F. Yang, X. Sun, X. Wang, W. Hu, Ternary NiCo2Px nanowires as pH-universal electrocatalysts for highly efficient hydrogen evolution reaction, Adv. Mater. 29 (2017) 1605502–1605507.
[25] Y. Shi, B. Zhang, Recent advances in transition metal phosphide nanomaterials: synthesis and applications in hydrogen evolution reaction, Chem. Soc. Rev. 45 (2016) 1529–1541.
[26] Z. Xing, Q. Liu, A.M. Asiri, X. Sun, Closely interconnected network of molybdenum phosphide nanoparticles: a highly efficient electrocatalyst for generating hydrogen from water, Adv. Mater. 26 (2014) 5702–5707.
[27] P. Xiao, M.A. Sk, L. Thia, X. Ge, R.J. Lim, J.-Y. Wang, K.H. Lim, X. Wang, Molybdenum phosphide as an efficient electrocatalyst for the hydrogen evolution reaction, Energy Environ. Sci. 7 (2014) 2624–2629.
[28] Z. Pu, S. Wei, Z. Chen, S. Mu, Flexible molybdenum phosphide nanosheet array electrodes for hydrogen evolution reaction in a wide pH range, Appl. Catal. B 196 (2016) 193–198.
[29] Y. Zhu, G. Chen, X. Xu, G. Yang, M. Liu, Z. Shao, Enhancing electrocatalytic activity for hydrogen evolution by strongly coupled molybdenum nitride@nitrogen-doped carbon porous nano-octahedrons, ACS Catal. 7 (2017) 3540–3547.
[30] X. Zou, Y. Zhang, Noble metal-free hydrogen evolution catalysts for water splitting, Chem. Soc. Rev. 44 (2015) 5148–5180.
[31] J. Xiong, W. Cai, W. Shi, X. Zhang, J. Li, Z. Yang, L. Feng, H. Cheng, Salt-templated synthesis of defect-rich MoN nanosheets for boosted hydrogen evolution reaction, J. Mater. Chem. A 5 (2017) 24193–24198.
[32] B. Cao, G.M. Veith, J.C. Neuefeind, R.R. Adzic, P.G. Khalifah, Mixed close-packed cobalt molybdenum nitrides as non-noble metal electrocatalysts for the hydrogen evolution reaction, J. Am. Chem. Soc. 135 (2013) 19186–19192.
[33] S. Gupta, N. Patel, R. Fernandes, R. Kadrekar, A. Dashora, A.K. Yadav, D. Bhattacharyya, S.N. Jha, A. Miotello, D.C. Kothari, Co–Ni–B nanocatalyst for efficient hydrogen evolution reaction in wide pH range, Appl. Catal. B 192 (2016) 126–133.
[34] K. Chang, H. Pang, X. Hai, G. Zhao, H. Zhang, L. Shi, F. Ichihara, J. Ye, Ultra-small freestanding amorphous molybdenum sulfide colloidal nanodots for highly efficient photocatalytic hydrogen evolution reaction, Appl. Catal. B 232 (2018) 446–453.
[35] N.H. Attanayake, A.C. Thenuwara, A. Patra, Y.V. Aulin, T.M. Tran, H. Chakraborty, E. Borguet, M.L. Klein, J.P. Perdew, D.R. Strongin, Effect of intercalated metals on the electrocatalytic activity of 1T-MoS2 for the hydrogen evolution reaction, ACS Energy Lett. 3 (2018) 7–13.
[36] Q. Liu, X. Li, Q. He, A. Khalil, D. Liu, T. Xiang, X. Wu, L. Song, Gram-scale aqueous synthesis of stable few-layered 1T-MoS2: applications for visible-light-driven photocatalytic hydrogen evolution, Small 11 (2015) 5556–5564.
[37] Y. Yin, J. Han, Y. Zhang, X. Zhang, P. Xu, Q. Yuan, L. Samad, X. Wang, Y. Wang, Z. Zhang, P. Zhang, X. Cao, B. Song, S. Jin, Contributions of phase, sulfur vacancies, and edges to the hydrogen evolution reaction catalytic activity of porous molybdenum disulfide nanosheets, J. Am. Chem. Soc. 138 (2016) 7965–7972.

[38] Y. Yu, G.-H. Nam, Q. He, X.-J. Wu, K. Zhang, Z. Yang, J. Chen, Q. Ma, M. Zhao, Z. Liu, F.-R. Ran, X. Wang, H. Li, X. Huang, B. Li, Q. Xiong, Q. Zhang, Z. Liu, L. Gu, Y. Du, W. Huang, H. Zhang, High phase-purity 1T′-MoS2- and 1T′-MoSe2-layered crystals, Nat. Chem. 10 (2018) 638–643.
[39] M.A. Lukowski, A.S. Daniel, F. Meng, A. Forticaux, L. Li, S. Jin, Enhanced hydrogen evolution catalysis from chemically exfoliated metallic MoS2 nanosheets, J. Am. Chem. Soc. 135 (2013) 10274–10277.
[40] Y. Yin, Y. Zhang, T. Gao, T. Yao, X. Zhang, J. Han, X. Wang, Z. Zhang, P. Xu, P. Zhang, X. Cao, B. Song, S. Jin, Synergistic phase and disorder engineering in 1T-MoSe2 nanosheets for enhanced hydrogen-evolution reaction, Adv. Mater. 29 (2017) 1700311.
[41] M.S. Faber, R. Dziedzic, M.A. Lukowski, N.S. Kaiser, Q. Ding, S. Jin, High-performance electrocatalysis using metallic cobalt pyrite (CoS2) micro- and nanostructures, J. Am. Chem. Soc. 136 (2014) 10053–10061.
[42] M.A. Lukowski, A.S. Daniel, C.R. English, F. Meng, A. Forticaux, R.J. Hamers, S. Jin, Highly active hydrogen evolution catalysis from metallic WS2 nanosheets, Energy Environ. Sci. 7 (2014) 2608–2613.
[43] Y. Yin, P. Miao, Y. Zhang, J. Han, X. Zhang, Y. Gong, L. Gu, C. Xu, T. Yao, P. Xu, Y. Wang, B. Song, S. Jin, Significantly increased raman enhancement on MoX2 (X = S, Se) monolayers upon phase transition, Adv. Funct. Mater. 27 (2017) 1606694.
[44] L. Wang, X. Liu, J. Luo, X. Duan, J. Crittenden, C. Liu, S. Zhang, Y. Pei, Y. Zeng, X. Duan, Self-optimization of the active site of molybdenum disulfide by an irreversible phase transition during photocatalytic hydrogen evolution, Angew. Chem. Int. Ed. 56 (2017) 7610–7614.
[45] Z. Wang, Y. Shen, Y. Ito, Y. Zhang, J. Du, T. Fujita, A. Hirata, Z. Tang, M. Chen, Synthesizing 1T–1H two-phase Mo1–xWxS2 monolayers by chemical vapor deposition, ACS Nano 12 (2018) 1571–1579.
[46] Y.C. Lin, D.O. Dumcenco, H.P. Komsa, Y. Niimi, A.V. Krasheninnikov, Y.S. Huang, K. Suenaga, Properties of individual dopant atoms in single-layer MoS2: atomic structure, migration, and enhanced reactivity, Adv. Mater. 26 (2014) 2857–2861.
[47] D. Voiry, A. Mohite, M. Chhowalla, Phase engineering of transition metal dichalcogenides, Chem. Soc. Rev. 44 (2015) 2702–2712.
[48] Y.-C. Lin, D.O. Dumcenco, Y.-S. Huang, K. Suenaga, Atomic mechanism of the semiconducting-to-metallic phase transition in single-layered MoS2, Nat. Nanotechnol. 9 (2014) 391.
[49] H. Li, S. Chen, X. Jia, B. Xu, H. Lin, H. Yang, L. Song, X. Wang, Amorphous nickel-cobalt complexes hybridized with 1T-phase molybdenum disulfide via hydrazine-induced phase transformation for water splitting, Nat. Commun. 8 (2017) 15377.
[50] J. Heising, M.G. Kanatzidis, Exfoliated and restacked MoS2 and WS2: ionic or neutral species? Encapsulation and ordering of hard electropositive cations, J. Am. Chem. Soc. 121 (1999) 11720–11732.
[51] Y. Li, K.-A.N. Duerloo, K. Wauson, E.J. Reed, Structural semiconductor-to-semimetal phase transition in two-dimensional materials induced by electrostatic gating, Nat. Commun. 7 (2016) 10671.
[52] Y. Wang, J. Xiao, H. Zhu, Y. Li, Y. Alsaid, K.Y. Fong, Y. Zhou, S. Wang, W. Shi, Y. Wang, A. Zettl, E.J. Reed, X. Zhang, Structural phase transition in monolayer MoTe2 driven by electrostatic doping, Nature 550 (2017) 487.
[53] C. Zhang, S. Kc, Y. Nie, C. Liang, W.G. Vandenberghe, R.C. Longo, Y. Zheng, F. Kong, S. Hong, R.M. Wallace, K. Cho, Charge mediated reversible metal–Insulator transition in monolayer MoTe2 and WxMo1–xTe2 alloy, ACS Nano 10 (2016) 7370–7375.
[54] J. Zhu, Z. Wang, H. Yu, N. Li, J. Zhang, J. Meng, M. Liao, J. Zhao, X. Lu, L. Du, R. Yang, D. Shi, Y. Jiang, G. Zhang, Argon plasma induced phase transition in monolayer MoS2, J. Am. Chem. Soc. 139 (2017) 10216–10219.
[55] Y. Tang, Z. Zhao, Y. Wang, Y. Dong, Y. Liu, X. Wang, J. Qiu, Carbon-stabilized interlayer-expanded few-layer MoSe2 nanosheets for sodium ion batteries with enhanced rate capability and cycling performance, ACS Appl. Mater. Inter. 8 (2016) 32324–32332.
[56] K. Qu, Y. Wang, A. Vasileff, Y. Jiao, H. Chen, Y. Zheng, Polydopamine-inspired nanomaterials for energy conversion and storage, J. Mater. Chem. A Mater. Energy Sustain. (2018).
[57] X. Hu, Y. Li, G. Zeng, J. Jia, H. Zhan, Z. Wen, Three-dimensional network architecture with hybrid nanocarbon composites supporting few-layer MoS2 for lithium and sodium storage, ACS Nano 12 (2018) 1592–1602.
[58] T. Hongjie, W. Jiangyan, Y. Huajie, Z. Huijun, W. Dan, T. Zhiyong, Growth of polypyrrole ultrathin films on MoS2 monolayers as high-performance supercapacitor electrodes, Adv. Mater. 27 (2015) 1117–1123.
[59] Z. Jintao, Q. Liangti, S. Gaoquan, L. Jiangyong, C. Jianfeng, D. Liming, N,P-codoped carbon networks as efficient metal-free bifunctional catalysts for oxygen reduction and hydrogen evolution reactions, Angew. Chem. Int. Ed. 55 (2016) 2230–2234.
[60] G. Ma, K. Huang, J.-S. Ma, Z. Ju, Z. Xing, Q.-c. Zhuang, Phosphorus and oxygen dual-doped graphene as superior anode material for room-temperature potassium-ion batteries, J. Mater. Chem. A 5 (2017) 7854–7861.
[61] Y. Haijing, T. Chungui, W. Lei, W. Aiping, M. Meichen, Z. Lu, F. Honggang, Phosphorus-modified tungsten nitride/reduced graphene oxide as a high--performance, non-noble-metal electrocatalyst for the hydrogen evolution reaction, Angew. Chem. Int. Ed. 54 (2015) 6325–6329.
[62] M. Chatti, T. Gengenbach, R. King, L. Spiccia, A.N. Simonov, Vertically aligned interlayer expanded MoS2 nanosheets on a carbon support for hydrogen evolution electrocatalysis, Chem. Mater. 29 (2017) 3092–3099.
[63] M.-Y. Li, Y. Shi, C.-C. Cheng, L.-S. Lu, Y.-C. Lin, H.-L. Tang, M.-L. Tsai, C.-W. Chu, K.-H. Wei, J.-H. He, W.-H. Chang, K. Suenaga, L.-J. Li, Epitaxial growth of a monolayer WSe2-MoS2 lateral p-n junction with an atomically sharp interface, Science 349 (2015) 524–528.
[64] D. Escalera-López, Y. Niu, S.J. Park, M. Isaacs, K. Wilson, R.E. Palmer, N.V. Rees, Hydrogen evolution enhancement of ultra-low loading, size-selected molybdenum sulfide nanoclusters by sulfur enrichment, Appl. Catal. B 235 (2018) 84–91.
[65] K. Qu, Y. Zheng, Y. Jiao, X. Zhang, S. Dai, S.-Z. Qiao, Polydopamine-inspired, dual heteroatom-doped carbon nanotubes for highly efficient overall water splitting, Adv. Energy Mater. 7 (2017) 1602068.
[66] K. Qu, Y. Zheng, X. Zhang, K. Davey, S. Dai, S.Z. Qiao, Promotion of electrocatalytic hydrogen evolution reaction on nitrogen-doped carbon nanosheets with secondary heteroatoms, ACS Nano 11 (2017) 7293–7300.